ADVANCED MATERIALS
www.advmat.de

Mimicking Antioxidases and Hyaluronan Synthase: A Zwitterionic Nanozyme for Photothermal Therapy of Osteoarthritis

Peng Yu, Yanyan Li, Hui Sun, Hongbo Zhang, Han Kang, Peng Wang, Qiangwei Xin, Chunmei Ding, Jing Xie, and Jianshu Li**

Restoring joint homeostasis is crucial for relieving osteoarthritis (OA). Current strategies are limited to unilateral efforts in joint lubrication, inhibition of inflammation, free radicals scavenging, and cartilage regeneration. Herein, by modifying molybdenum disulfide (MoS_2) with Mg^{2+}-doped polydopamine and coating with polysulfobetaines, a dual-bionic photothermal nanozyme (MPMP) is constructed to mimic antioxidases/hyaluronan synthase for OA therapy. Photothermally enhanced lubrication lowers the coefficient of friction (0.028) in the early stage of OA treatment. The antioxidases-mimicking properties of MPMP nanozyme contribute to eliminating reactive oxygen and nitrogen species (ROS/RNS) (over 90% of scavenging ratio for H_2O_2/·OH/$O^{\cdot}{}_2^-$/DPPH/$ABTS^+$) and supplying O_2. With NIR irradiation, the MPMP nanozyme triggers thermogenesis (upregulating HSP70 expression) and Mg^{2+} release, which promotes the chondrogenesis in inflammatory conditions by deactivating NF-κB/IL-17 signaling pathways and enhancing MAPK signaling pathway. Benefiting from HSP70 and Mg^{2+}, MPMP-NIR shows HAS-mimicking activity to increase the intracellular (twofold) and extracellular (3.12-fold) HA production. Therefore, MPMP-NIR demonstrates superior spatiotemporally therapeutic effect on OA in mice model, in terms of osteophytes (83.41% of reduction), OARSI scores (88.57% of reduction), and ACAN expression (2.70-fold of increment). Hence, insights into dual-bionic nanozymes can be a promising strategy for OA therapy or other inflammation-related diseases.

1. Introduction

Osteoarthritis (OA) is a chronic disease characterized by cartilage degeneration.[1] The growing inflammatory response, overproduced reactive oxygen/nitrogen species (ROS/RNS), and abnormal friction forces imperil the structures and functions of joint cartilage.[1,2] Recently, several new therapeutic strategies including viscosupplementation[3] and intra-articular injection of lubricants[4] and active species,[5] have been proposed for OA treatment. They have improved the outcomes of OA, however, OA cartilage is still regarded as an incurable tissue and has a tendency to relapse, and finally develop into chondronecrosis. The difficulty in self-generation of cartilage involves its avascular/aneural features, which limit the growth and proliferation of chondrocytes.[6] Notably, the growth plates of children also have relatively poor vessels; whereas they provide a superior growth environment for chondrocytes.[7] In this area, heat shock protein 70 (HSP70) is continuously expressed at relatively higher levels compared to other tissues.[8] Whether stimulating the

P. Yu, H. Sun, H. Zhang, P. Wang, Q. Xin, C. Ding, J. Xie, J. Li
College of Polymer Science and Engineering
State Key Laboratory of Polymer Materials Engineering
Sichuan University
Chengdu 610065, P. R. China
E-mail: xiej@scu.edu.cn; jianshu_li@scu.edu.cn

Y. Li
School of Chemistry and Chemical Engineering
Shanxi University
Taiyuan 030006, P. R. China

H. Kang
Life Science Core Facilities
College of Life Sciences
Sichuan University
Chengdu 610065, P. R. China

J. Li
State Key Laboratory of Oral Diseases
West China Hospital of Stomatology
Med-X Center for Materials
Sichuan University
Chengdu 610041, P. R. China

The ORCID identification number(s) for the author(s) of this article can be found under https://doi.org/10.1002/adma.202303299

DOI: 10.1002/adma.202303299

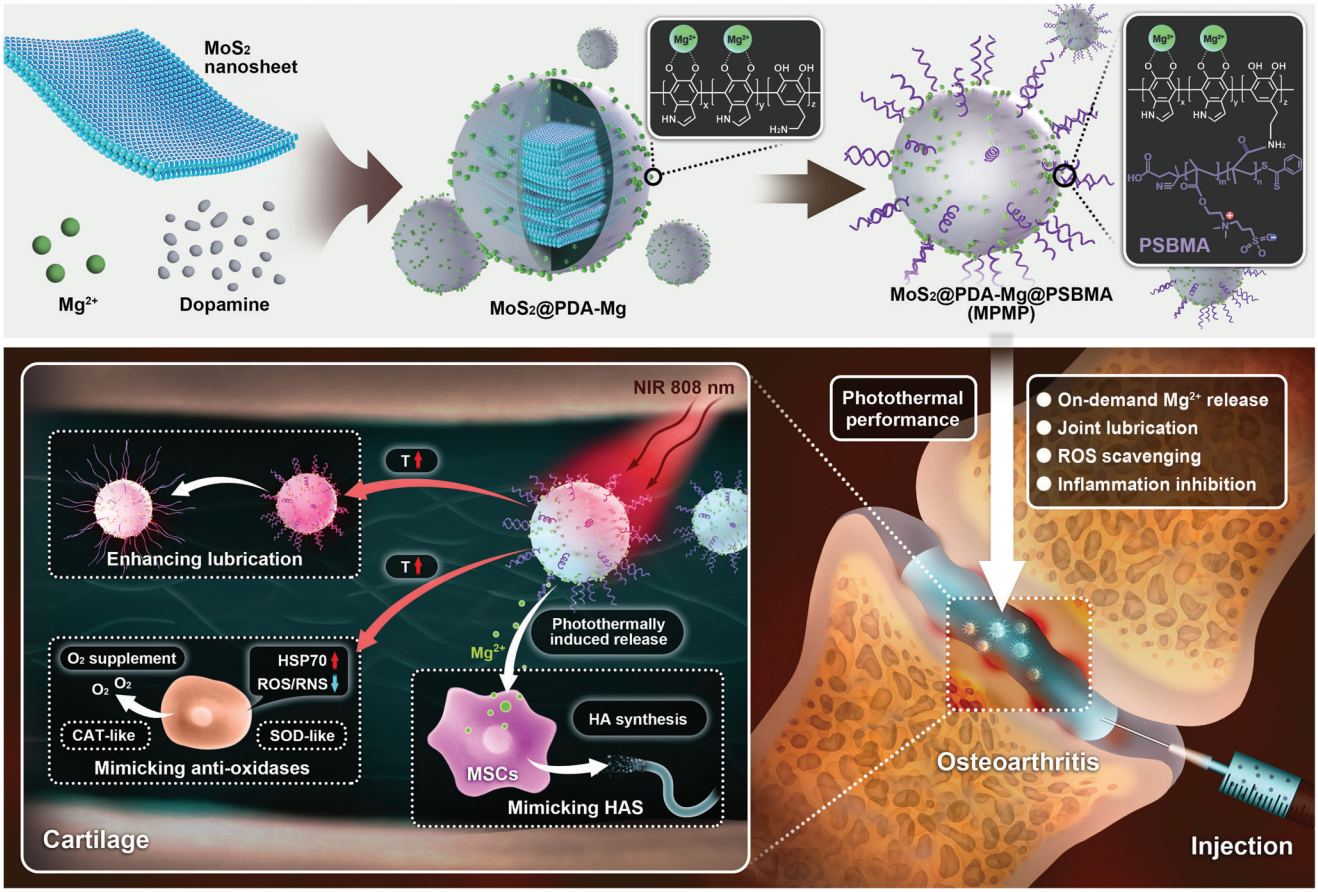

Scheme 1. Schematic diagram of the fabrication procedures and therapeutic mechanism for OA of MPMP nanozyme based on the joint lubrication, antioxidases-mimicking abilities to scavenge reactive species and supply O_2, and HAS-mimicking ability to polymerize HA.

expression of HSP70 can promote chondrogenesis and further improve the therapeutic effect of OA has not yet been reported.

Photothermal therapy (PTT) is widely used for the treatment of cancer,[9] OA,[10] and some bone-related diseases.[11] However, PTT-induced HSP70 expression in OA therapy is still rare. Among various photothermal biomaterials, 2D molybdenum disulfide (MoS_2) nanosheets can be regarded as popular candidates for OA therapy owing to three definite advantages: the photothermal conversion property, specific lubrication, and enzymatic performance, such as superoxide dismutase (SOD)-mimicking and catalase (CAT)-mimicking activities to scavenge ROS.[12] To improve the photothermal conversion efficiency (PCE), decoration with polydopamine (PDA) and its analogs is often applied owing to their broad light absorption (especially within the near-infrared region of 700–1300 nm),[13] along with excellent intrinsic antioxidation properties.[14]

Nanozymes are nanomaterials provided with enzyme-like properties, which are a kind of artificial enzymes.[15–17] In recent years, there are some nanozyme materials have been utilized to treat arthritis.[15,16] For example, MoS_2-based, PDA-based, MnO_2-based, and CeO_2-based have exhibited outstanding capacities in inhibiting inflammation and scavenging ROS, and some nanozymes could also exhibit photothermal conversion ability.[18–21] However, the therapeutic effect relies on the inflammation-inhibition drugs or chondroinducive agents, and little is known the intrinsic capacity of nanozyme to stimulate the self-generation of cartilage.

Hyaluronic acid (HA), which is important for joint homeostasis owing to its joint lubrication, viscosity supplement, and anti-inflammatory properties,[22] is mainly biosynthesized by hyaluronan synthase 2 (HAS 2).[23] Nevertheless, overexpressed hyaluronidase and ROS in OA would degrade HA and inhibit HAS expression, thereby causing dysfunction of both joint cartilage and synovial fluid.[24] Although diverse strategies such as HAS-based controlled delivery system and HA-mimicking biomaterials have attracted much scientific attention,[6,25] there is also a gap in the development of artificial HAS to trigger endogenous HA biosynthesis to alleviate OA.

In this study, we designed a MoS_2-based nanozyme with stepwise modification of Mg^{2+}-doped polydopamine and zwitterionic polysulfobetaine (MoS_2@PDA-Mg@PSB, MPMP) (**Scheme 1**), which was used for the photothermal therapy of OA. The dual-bionic performances (mimicking antioxidases and HAS) were enhanced by synergistic effect of the upregulation of HSP70 expression and on-demand release of Mg^{2+} release, which were attributed to the mild thermogenesis from photothermal effect; thus, MPMP-NIR promoted the chondrogenic differentiation of bone marrow mesenchymal stem cells (BMSCs) and enhanced HA production by synovial mesenchymal stem cells (SMSCs) in inflammatory microenvironments. The MIA animal model

further indicated an excellent cartilage repair effect, demonstrating that combining HAS-mimicking and antioxidases-mimicking activities into a zwitterionic nanozyme system exhibits good feasibility for the catalytic therapy of OA.

2. Results and Discussion

2.1. Synthesis and Characterizations of the Dual-Enzyme-Mimicking MPMP Nanozyme

To fabricate an MPMP nanozyme that mimics antioxidases/HAS, PSBMA-*b*-PNHSMA (PSN) was first synthesized by RAFT polymerization (Scheme S1, Supporting Information), which is a diblock copolymer containing zwitterionic sulfobetaine moiety and an active ester moiety (NHS ester). Concurrently, MoS_2 nanosheets modified with Mg^{2+}-doped polydopamine (MPM) were fabricated by a "one-pot" method. Finally, PSN was grafted onto the MPM nanozyme by amidation to prepare MPMP nanozymes (**Figure 1**a).

NHSMA was successfully synthesized prior to RAFT polymerization. The peaks at 5.87 and 6.41 ppm refer to the carbon–carbon double bond of methyl-acrylic moieties (Figure S1, Supporting Information) according to ^{1}H NMR. The chemical structure is further confirmed by the ^{13}C NMR (Figure S1b, Supporting Information). Moreover, the typical peaks at 998, 1632, and 3005 cm^{-1} belong to the double bond (CH_2═C(CH_3)—), and the peaks at 1982 and 2006 cm^{-1} prove the existence of the NHS ester (Figure S2, Supporting Information). The m/z value (183) in MS spectra (Figure S3, Supporting Information) is close to the theoretical value (183.05), which further confirms the successful synthesis of NHSMA. Next, a zwitterionic sulfobetaine homopolymer (PSBMA-macroCTA, PSB) was synthesized as a macromolecular CTA-initiator to prepare PSN diblock copolymers. As shown in Figure 1b, the disappearance of the double bonds of SBMA and NHAMA confirms successful polymerization, and the ratio of zwitterion/active ester is close to 10/1. This diblock copolymer is hydrophilic in an ionic solution, and the reactive NHS groups can react with amine (—NH_2) from polydopamine in the current study.

The ultrasonic method was applied to fabricate the MoS_2 nanosheets. Then, a metal–oxygen coordination bond between MoS_2/Mg^{2+} and PDA was generated to prepare the MPM nanozyme. Subsequently, zwitterionic PSN was conjugated to the MPM nanozyme in a weakly basic solution (pH 8.5). In contrast to the original lamellar structures of the MoS_2 nanosheets, the decoration of Mg^{2+}-doped PDA and grafting of zwitterionic polymers exhibit obvious organic layers (Figures S4a and S5a, Supporting Information, Figure 1c). According to the high-resolution transmission electron microscopy (TEM) images, the decoration of Mg^{2+}-doped PDA and zwitterionic PSB does not affect the lattice fringe, which corresponds to the (002) plane of MoS_2 (Figures S4b and S5b, Supporting Information, Figure 1d). The main elements of the MoS_2 nanosheets (Mo and S) are surrounded by the major elements of PDA-Mg and PSB (C, N, O, Mg), and a uniform distribution of Mg is also observed in MPM and MPMP nanozymes (Figures S4c and S5c, Supporting Information, Figure 1e), indicating the embedding of MoS_2 in the organic layers. The XRD pattern implies the main plane of (002) (2θ = 14°), which is indexed to 2H-MoS_2, and the MPM and MPMP nanozymes do not affect the crystal structure of the inner MoS_2 (Figure 1f).

FT-IR, Raman, and XPS spectroscopies were used to characterize the chemical structures of MoS_2, MPM, and MPMP nanozymes. Two distinct bands at 464 and 641–645 cm^{-1} reveal the successful fabrication of MoS_2 nanosheets and chemical stability in the modification processes (Figure S6, Supporting Information). The additional characteristic bands at 1388 (or 1384) cm^{-1} and 1599 (or 1603) cm^{-1} refer to the stretching vibrations from the phenol groups and aromatic rings from PDA. According to FT-IR spectra, the appearance of 1039 cm^{-1}referring to the stretching vibration from the sulfonate groups and disappearance of 1800/1777 cm^{-1} referring to the cyclic amide group, verify the successful conjugation of PSN to MPM nanozyme through an amide reaction between the amine groups of PDA and active ester groups of PSN (Figure 1g). XPS analysis shows that the Mo element in MoS_2, MPM, and MPMP nanozymes has two covalent states: Mo^{6+} ($Mo^{6+}3d_{3/2}$) and Mo^{4+} ($Mo^{4+}3d_{5/2}$ and $Mo^{4+}3d_{5/2}$) (Figure 1h; Figure S7, Supporting Information), which exhibits as the redox couple enables their potential to scavenge free radicals.[26,27] With the decoration of Mg^{2+}-doped polydopamine, there is obviously an increased ratio of [C]/[Mo] and the appearance of Mg element (Figure S8 and Table S1, Supporting Information). The increased ratio of [S]/[Mo] indicates the success of the PSB conjugation. Although there is a loss of Mg^{2+} during the process of polymer conjugation, which is proved by the reduced ratio of [Mg]/[Mo], it has no adverse effect on the performance of the following dual-bionic nanozyme performances. When Mg^{2+} have been introduced in the process of fabrication of PDA-based nanomaterials, several hydrogen bonds between phenol groups in PDA (1340 cm^{-1}) and MoS_2@polydopamine (MP, 1338 cm^{-1}) has been influenced, thus the blueshifted peaks at 1365 and 1364 cm^{-1} have appeared in PDA-Mg and MPM groups, respectively (Figure S9, Supporting Information), There are obvious phenol-Mg^{2+} bonds in the high XPS resolution spectra of O1s and Mg1s of MPM and MPMP nanozymes (Figure S10, Supporting Information), which further confirm the coordination between Mg^{2+} and phenol groups. Furthermore, only MPM and MPMP nanozymes show a peak at 280 nm, which is absent in the PSN polymer and MoS_2 nanosheets, further demonstrating the presence of PDA (Figure S11, Supporting Information). With the decoration of the organic component, the MPM and MPMP nanozymes exhibit larger hydrodynamic diameters (D_h) than the MoS_2 nanosheets, and the MPMP nanozyme shows the largest particle size owing to the hydration ability of the zwitterionic polymer (Figure S12a–f, Supporting Information). The nanoscale hydrodynamic diameters of three nanozymes are fundamental for intra-articular injection. In saline, the D_h of MoS_2 nanosheets increases slightly at 2 and 7 days, whereas there are obvious differences in D_h and precipitation of MPM solution when incubated at 37 °C for 2 and 7 days (Figure S12g, Supporting Information). As for DMEM system, the D_h of three nanozymes is larger than that in saline, which could be attributed to the adsorption of amino acids, vitamin, and glucose, and the changes in the particle sizes of MoS_2 nanosheets and MPM nanozyme are more obvious. Fortunately, MPMP nanozyme shows relatively stable D_h in both saline and DMEM, indicating that modification of zwitterionic polymers could inhibit the aggregation of the MPMP nanozyme, thus improving its stability in

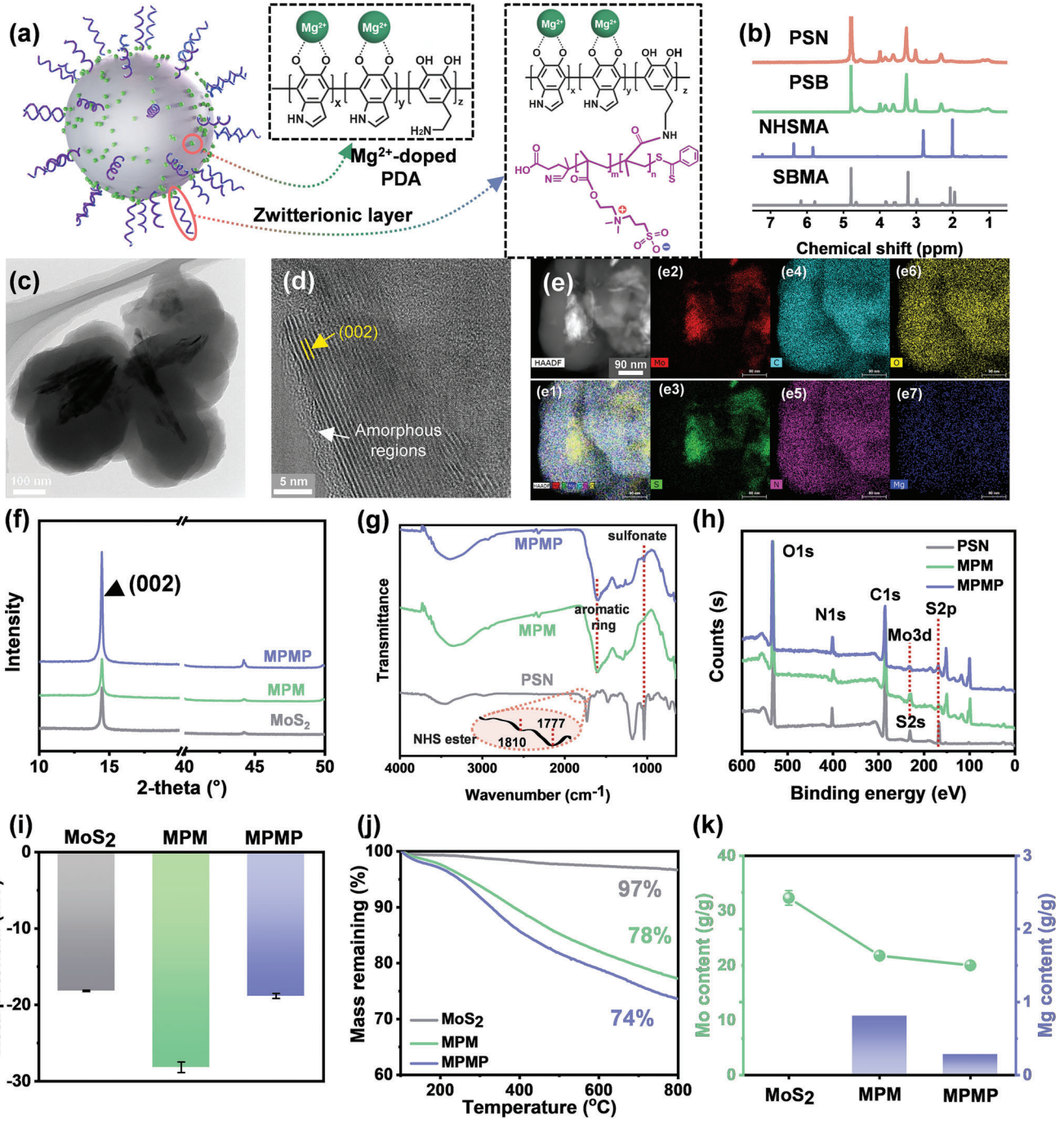

Figure 1. a) Scheme of MPMP nanozyme and the chemical structures of Mg^{2+}/MoS_2-incorporated PDA and zwitterionic PSN. b) ^1H NMR spectra of SBMA, NHSMA, PSB, and PSN. c) Low- and d) high-resolution TEM images of MPMP nanozyme, e) High-angle annular dark-field scanning transmission microscopy (HAADF-STEM) image and corresponding elemental mappings of the merged image (e1), Mo (e2), S (e3), C (e4), N (e5), O (e6), and Mg (e7). f) XRD spectra of MPMP nanozyme. g) FT-IR spectra of PSN, MPM, and MPMP. h) XPS analysis of MPMP nanozyme. i) Zeta potential, j) TGA curve, and k) element analysis (Mo and Mg) by inductively coupled plasma (ICP) of MoS_2, MPM, and MPMP nanozyme. Data are shown as mean ± SD ($n = 3$).

physiological conditions. Moreover, MPMP nanozyme has maintained the original structures after a 7-day incubation in saline (Figure S13, Supporting Information). Therefore, MPMP nanozyme can be prepared as powder samples and then dispersed in saline through ultrasonicatio methods for several minutes, which could better avoid the aggregation of nanozymes in the future applications. After decoration of Mg^{2+}-doped PDA, MPM shows higher negative charge (−28.16 mV) than MoS_2 (−18.17 mV), while the zeta potential of MPMP nanozyme reduces to −18.83 mV (Figure 1i) because the

neutralization of sulfobetaine polymers could weaken the negative charge of phenols from PDA. As the organic contents increases, remaining mass at 600 °C decreases from 97% (MoS_2) to 78% (MPM) and 74% (MPMP) (Figure 1j). Similarly, the Mo content of the composite nanozymes is lower than that of MoS_2 (Figure 1k). There is 0.81 g/g of Mg^{2+} in the MPM nanozyme, while it reduces 65% in MPMP nanozyme, which is in accordance with the results of XPS. Overall, all the data indicate the successful fabrication of MPMP nanozyme.

2.2. Photothermal Performance of the MPMP Nanozyme

Arising from the photothermal conversion capacity of MoS_2 (denoted as M nanozyme hereafter) and PDA, the MPMP nanozyme can produce heat with the irradiation of an 808 nm laser. The heating rate and final temperature improvement are positively correlated to the irradiation power density from 0.2 to 2.0 W cm^{-2} (**Figure 2**a). Without modification of Mg^{2+}-doped PDA, MoS_2 nanosheets exhibit limited heating performance even at a concentration of 100 μg mL^{-1} (Figure S14, Supporting Information). Although the final temperature at 15 min increases gradually with enhanced irradiation power density from 0.2 to 2.0 W cm^{-2}, relatively higher power density (at least 1.5 W cm^{-2}) is required to reach 40 °C. MPM and MPMP nanozymes have better photothermal effects with the introduction of Mg^{2+}-doped PDA (Figure S15, Supporting Information, Figure 2b,c), as PDA is regarded as an ideal artificial melanin owing to its excellent photothermal conversion efficiency.[28] Higher irradiation power densities (1.5 and 2.0 W cm^{-2}) for MPM and MPMP nanozymes have resulted in excessive temperature (>45 °C), which is not suitable for OA therapy. In detail, thermal stimulation of 43 °C would have an adverse effect on the viability and metabolism of chondrocyte-like cell lines.[29] Temperature over 45 °C would lead to lower viability of chondrocytes, de-organization of growth-plate, and over expression of TNF-α.[30] Even worse, thermal stimulus at 48 °C could induce apoptosis of chondrocytes and inhibition of biosynthesis of proteoglycan.[31] Conjugation of zwitterionic polymer has merely affected the photothermal conversion performance of MPMP nanozymes slightly; however, its final temperature at ≈40 °C (1.0 W cm^{-2}, 100 μg mL^{-1}) is desirable to promote tissue regeneration.[11,32] Based on the above data, a 1.0 W cm^{-2} of power density and 100 μg mL^{-1} of MPMP nanozyme concentration were appropriate for the following in vitro and in vivo studies.

According to five repeated "heating/cooling" cyclic measurements, no decay in the temperature change is observed (Figure 2d), suggesting good photothermal stability. Based on previous studies,[33] the photothermal conversion efficiencies (PCE) of M, MPM, and MPMP nanozymes are calculated as 12.35%, 43.07%, and 36.40%, respectively (Figure 2e). When MoS_2 nanosheets are absent, the corresponding PDA (P), PDA-Mg (PM), and PDA-Mg@PSBMA (PMP) nanoparticles exhibited better photothermal behaviors and higher PCE (55.08% for P, 48.01% for PM and 47.50% for PMP) (Figure S16, Supporting Information), indicating that polydopamine contributes more to photothermal conversion than MoS_2 nanosheets. However, the final temperatures of P, PM, and PMP nanozymes were over 50 °C, which is harmful to cell survival. Therefore, the introduction of MoS_2 nanosheets benefits to the bimedical applications of MPMP nanozyme. Thermogenesis is a common strategy for supplying energy to promote the molecular motion, thereby promoting the release kinetics in numerous drug delivery systems.[34] Obviously, Mg^{2+} is intelligently released from the MPMP nanozyme in an on-demand manner (Figure 2f), demonstrating that Mg^{2+} release can be controlled through an 808 nm laser. Moreover, intra-articulate (I.A.) injection of M, MPM, and MPMP nanozymes followed by irradiation at 808 nm directly was utilized to characterize the local heat production at the knee joint (Figure 2g). Unlike the virtually unanimous joint temperature after saline injection and M nanozyme, administration of MPMP nanozyme could conduct nearly 10 °C of temperature increment (Figure 2h), which is fundamental for the subsequent PTT of OA. As for MPM nanozyme with the highest PCE, it doesn't trigger efficient heat generation in vivo. There are perhaps two reasons for the unsatisfactory in vivo photothermal performance of MPM nanozyme: i) some MPM nanozyme remains within the syringe due to the universal adhesion property of polydopamine, which reduced the final amount of MPM nanozyme in OA joints; ii) MPM absorbs abundant carbohydrate polymers and proteins, which lowers its light absorbance ability. The location sites (absorption on the surface or penetration in the deep zones of cartilage) of MPMP under NIR irradiation have been explored through an in vitro model (Figure S17a, Supporting Information). There is no difference in the cross-section images of the control group and MPMP group (Figure S17b,d, Supporting Information), whereas these are obvious MPMP nanozyme aggregates absorbed on the cartilage surfaces of MPMP groups (Figure S17e, Supporting Information), which differs from the clear cartilage surface of control group (Figure S17c, Supporting Information). In addition, the absorbed MPMP nanozyme would contribute to a slight temperature increment under NIR irradiation owing to its photothermal property (Figure S18, Supporting Information). Consequently, the MPMP nanozyme display excellent photothermal properties, making it a viable PTT biomaterial.

2.3. Photothermally Enhanced Lubrication Properties of MPMP Nanozyme

In the healthy joint, there are stable boundary layers on the cartilage superficial layer, thereby providing excellent lubrication performance to weaken the friction forces.[1,6] However, with the pathological process of OA, most cartilage components, including HA, Col II, and lubricin degrade gradually, thus impairing the lubricity of cartilage.[6] To evaluate the photothermal-mediated lubrication property, the MPMP nanozyme was subjected to a tribology test in a ball-to-plate model under NIR irradiation (Figure 2i). The MPMP nanozyme under the load force at 1 N exhibits a low dynamic coefficient of friction (COF, ≈0.031) (Figure 2j). With NIR irradiation, the dynamic COF (≈0.028) significantly decreases to 0.028 ($p < 0.05$), and a 30% reduction of the static COF has appeared ($p < 0.01$). Besides, they are stable with the shrinkage of the loading force, indicating the lubrication stability of the MPMP nanozyme under NIR irradiation. Charged $-N^+(CH_3)_2-$ and $-SO_3^{2-}$ groups are known to absorb water molecules via ion–dipole interactions to form a hydration

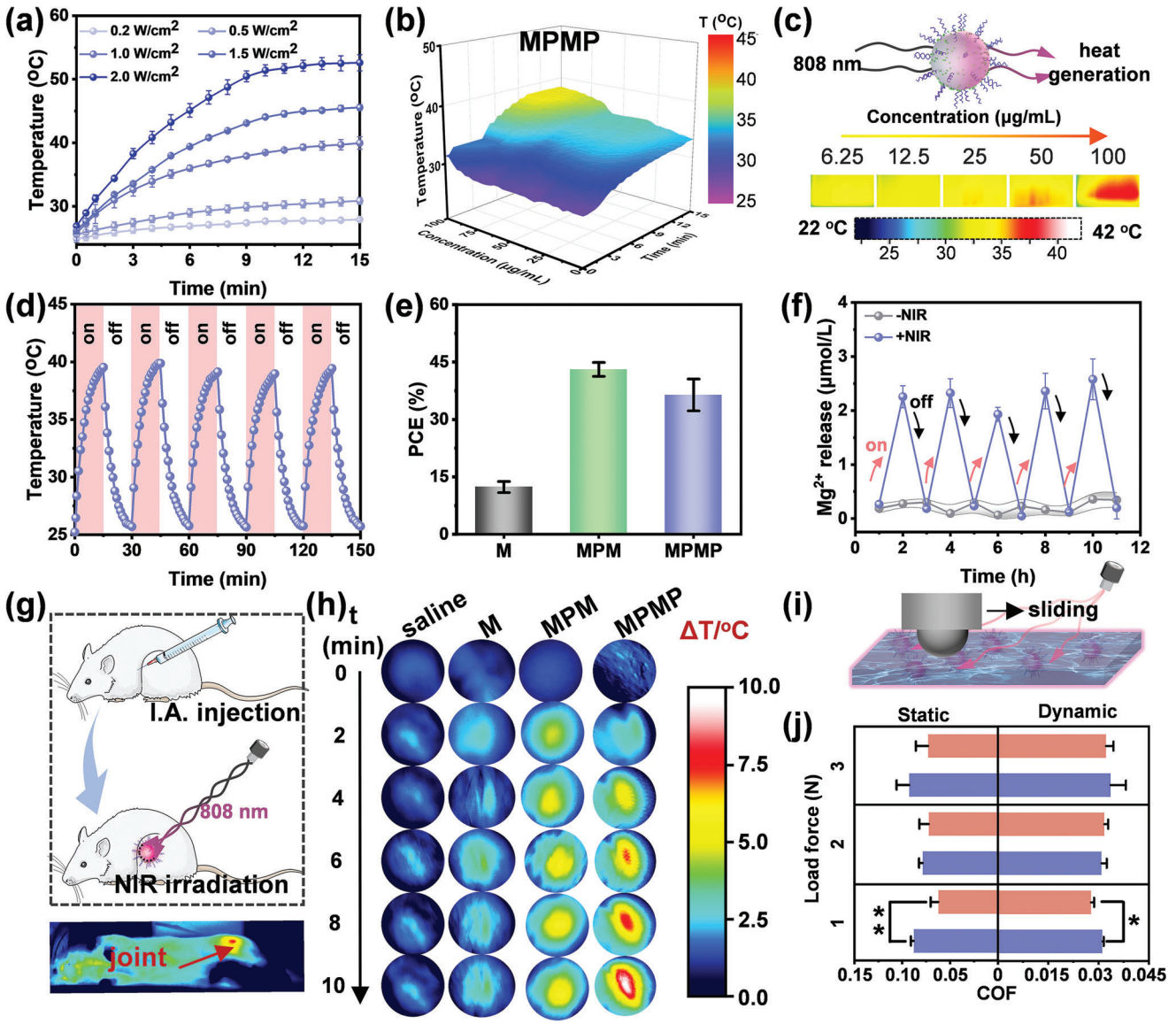

Figure 2. Photothermal conversion, on-demand Mg^{2+} release, and lubrication evaluation. a) Temperature-increment profiles of MPMP nanozyme under NIR irradiation of 0.2, 0.5, 1.0, 1.5, and 2.0 W cm^{-2} over 15 min. b) Temperature change of MPMP nanozyme with different nanozyme content and irradiation time. c) Visual photographs of final temperature of MPMP nanozyme (6.25–100 μg mL^{-1}) under NIR irradiation of 808 nm for 15 min. d) Temperature-change curves of MPMP nanozyme with five repeated "heating/cooling" NIR irradiation. e) Photothermal conversion efficiency of M, MPM, MPMP nanozymes. f) On-demand release profile of Mg^{2+} from MPM and MPMP nanozymes with or without NIR irradiation. g) Thermogenesis at joint site of MPMP with NIR irradiation and h) temperature change (0, 2, 4, 6, 8, and 10 min) of joint locally injected by saline, M, MPM, and MPMP nanozyme. i) Schematic illustration of lubrication test under NIR irradiation and j) static/dynamic COF of MPMP nanozyme. The orange and blue represent MPMP nanozyme with and without NIR irradiation. Data are shown as mean ± SD ($n = 3$). *($p < 0.05$) and **($p < 0.01$) suggest significant difference.

layer, which is crucial for hydration lubrication, however, it is inevitable that some side chains interact together through ionic interactions and hydrogen bonds, thereby imposing restrictions on hydration lubrication. Owing to the good photothermal effect, the thermogenesis of the MPMP nanozyme can provide enough energy to zwitterions to overcome the energy barriers of ionic interactions and hydrogen bonds; thus, more zwitterionic side chains are free to absorb water molecules and form a hydration layer. Overall, MPMP-NIR shows better lubrication performance than MPMP nanozyme itself.

2.4. Effect of Antioxidases-Mimicking MPMP Nanozyme on the Free Radicals Scavenging

In contrast to normal biological environments, inflamed joints are associated with overexpressed free radicals, such as ROS and RNS, followed by an unexpected invasion of joint cartilage, which induces cell damage and extracellular matrix (ECM) digestion.[35] Antioxidases inside the body are natural defense soldiers that eliminate ROS and RNS;[36] thus, it is of scientific significance to evaluate the antioxidases-mimicking activities

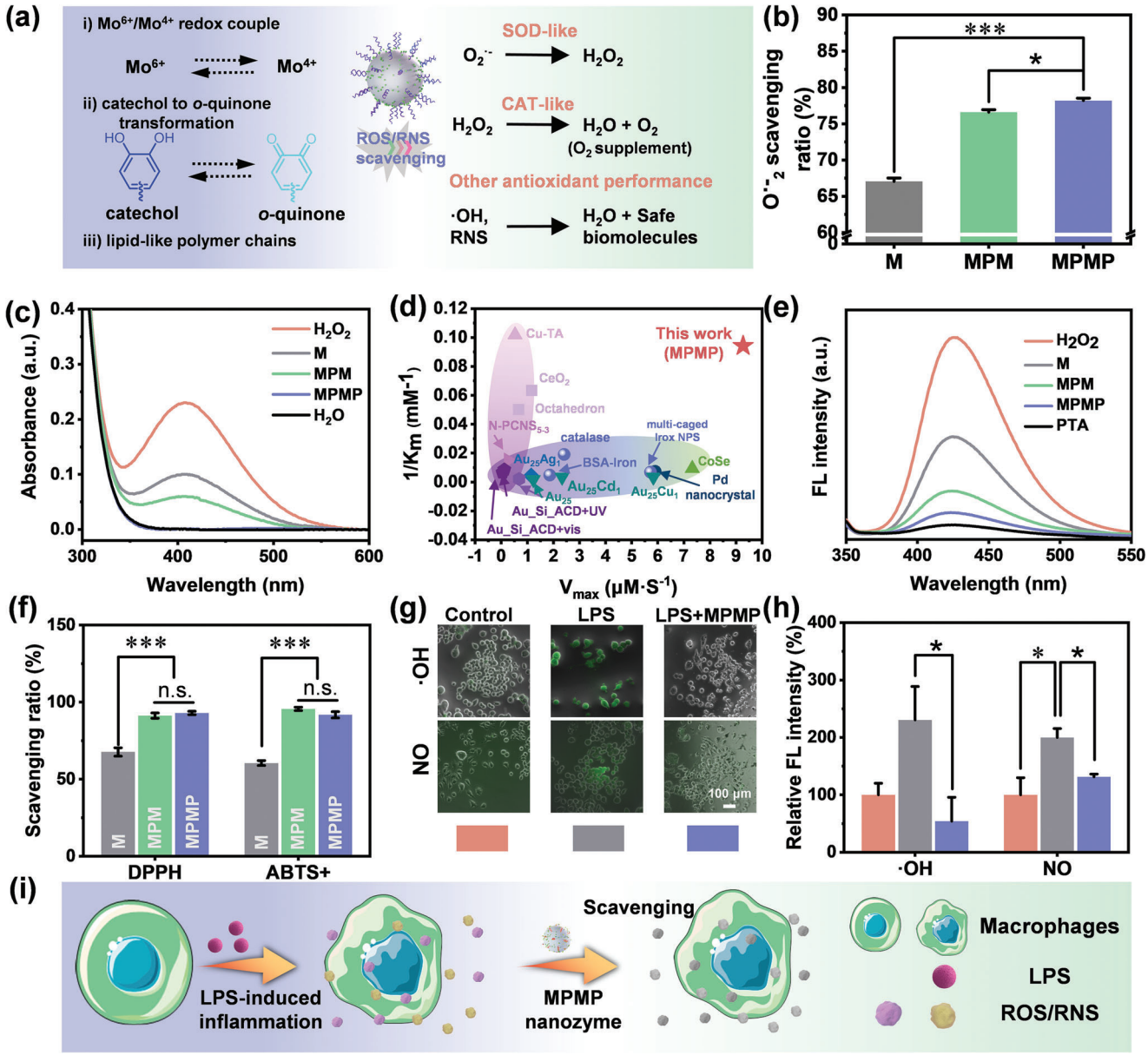

Figure 3. Antioxidases-mimicking performance of MPMP nanozyme. a) Schematic diagram of SOD-mimicking and CAT-mimicking capacities of MPMP nanozyme for ROS/RNS scavenging and O_2 supplement. b) $O^{\cdot}{}_2^-$ scavenging, and c) H_2O_2 scavenging ($Ti(SO_4)_2$ method) of M, MPM, and MPMP nanozymes. d) The CAT-mimicking catalytic parameters of MPMP nanozyme in comparison with other nano-catalysts, which are listed in Supporting Information in detail. e) The ·OH scavenging (PTA method) of M, MPM, and MPMP nanozymes. f) RNS scavenging effect of M, MPM, and MPMP nanozymes: DPPH and $ABTS^+$. g) Intracellular of ·OH and NO scavenging ability of MPMP nanozyme and h) corresponding quantitative analysis of fluorescence intensity. i) Scheme of inflammation induction and ROS/RNS scavenging of MPMP nanozyme. Data are shown as mean ± SD ($n = 3$). * ($p < 0.05$), and *** ($p < 0.001$) indicates a significant difference in comparison to the M group; * ($p < 0.05$) indicates statistical difference between MPM and MPMP groups and n.s. ($p > 0.05$) suggests that there is no statistical difference.

of MPMP nanozyme. Similar to MoS2-based, PDA-based and lipid-like materials,[18b] the antioxidases-mimicking performances of MPMP nanozyme, especially SOD-mimicking and CAT-mimicking activities, would finally scavenge ROS/RNS and supply O_2 (**Figure 3**a).

The SOD-mimicking activity of three nanozymes was evaluated based on their $O^{\cdot}{}_2^-$ scavenging performance. The $O^{\cdot}{}_2^-$ scavenging capacity of MPMP (78%) is higher than that of the M (67%) and MPM (76%) nanozymes (Figure 3b). On the other hand, OA joints exhibit an acidic microenvironment; thus, the SOD-mimicking activities in acidic conditions have been evaluated by FRAP. The results suggest that only MPMP nanozyme shows statistically higher antioxidant activity than MoS_2 ($p < 0.05$) (Figure S19, Supporting Information). These results reveal that decoration of the MoS_2 nanosheets with melanin-like Mg^{2+}-doped PDA contributes to higher SOD-mimicking activities to

scavenge ROS and introduction of zwitterionic polymers with lipid-like structures enhance antioxidation properties.

The CAT-mimicking activities are represented by H_2O_2 scavenging and O_2 generation properties. The scavenging of H_2O_2, which is regarded as one of the most stable ROS in OA joints, was evaluated through $Ti(SO_4)_2$ with an absorbance at 405 nm. As shown in Figure 3c, MPM and MPMP nanozymes present better H_2O_2 scavenging ability than MoS_2 nanosheets, and the H_2O_2 scavenging ratio of MPMP nanozyme is calculated to be 92.87% (Figure S20, Supporting Information), which is 1.46-fold and 1.86-fold that of MPM and M nanozymes, respectively. As expected, all nanozymes demonstrated CAT-mimicking catalytic effect, producing more O_2 than the natural decomposition of H_2O_2, and more O_2 bubbles are observed in the MPMP group (Figure S21, Supporting Information).

Naturally, SOD and CAT have conducted cascade antioxidative reactions: $O^{\cdot}{}_2^-$ is catalyzed to H_2O_2, and then the accumulated H_2O_2 is converted to H_2O and O_2. In terms of M, MPM, and MPMP nanozymes, their SOD-mimicking and CAT-mimicking catalytic kinetics were studied to calculate Michaelis–Menten constant (K_m) and the maximum initial velocity (V_{max}) using Lineweaver–Burk plots (Figures S22–S24, Supporting Information). As for the SOD-mimicking cytalytic process, there is no difference in the V_{max} of M, MPM, and MPMP nanozymes (Table S2, Sopporting Information). However, the K_m of MPMP nanozyme (314.75 μM) is lower than M nanozyme (327.35 μM), and MPMP nanozyme exhibits a 47.33% of reduction in K_m. These data imply that decoration with Mg^{2+}-doped polydopamine enhances the SOD-mimicking activity of nanozymes, and decoration of polysulfobetaine plays a vital role in improving the affinitiy of nanozyme to $O^{\cdot}{}_2^-$, thus, MPMP shows the highest SOD-mimicking catalytic activity for $O^{\cdot}{}_2^-$ scavenging. As for the H_2O_2 scavenging kinetics, the K_m of both M and MPM nanozymes are lower than those of the MPMP nanozyme (10.61 mM), indicating the highest affinity of MPMP toward H_2O_2. Moreover, most previous nano-catalysts could merely realize the high catalytic rate (V_{max}) or superior affinity to H_2O_2 ($1/K_m$) (Table S3, Supporting Information), whereas MPMP nanozyme exhibit higher V_{max} and $1/K_m$ at the same time (Figure 3d). Compared with M (2.13 mg L^{-1} s^{-1}) and MPM (2.26 mg L^{-1} s^{-1}) nanozymes, the MPMP nanozyme exhibits the highest catalytic kinetic parameters (2.65 mg L^{-1} s^{-1}) in O_2 generation, and MPMP nanozyme demonstrated the lowest K_m, indicating that MPMP has optimal CAT-mimicking activity to produce O_2 among these three nanozymes. Overall, MPMP exhibits the best SOD-mimicking and CAT-mimicking catalytic kinetics for the cascade ROS scavenging process.

·OH scavenging is also a common indicator to evaluate the antioxidation property of nanozymes. Gradual decreases in peak intensities are observed for the M-, MPM-, and MPMP-treated solutions (Figure 3e). Furthermore, the ·OH scavenging activity of three nanozymes shows concentration-dependent performance (Figure S25, Supporting Information), and the MPMP nanozyme at a concentration of 100 μg mL^{-1} exhibits a 93% of ·OH scavenging ratio, which is higher than that of M (53%) and MPM (82%). After the scavenging treatment, the residual ·OH are trapped by DMPO. As shown in Figure S26 (Supporting Information), DMPO–·OH (intensity ratio of 1:2:2:1) is obvious in the control group, whereas a sharp reduction in intensity appears in the M group, and there is almost no significant peak intensity in the MPM and MPMP groups owing to their relatively high scavenging ability.

DPPH is regarded as a typical molecule for evaluating the capacity of biomaterials in scavenging nitrogen free radicals (Figure S27a, Supporting Information). The violet DPPH solution fades after the treatment with MPMP nanozymes for 0.5 h (Figure S27b, Supporting Information), and the absorbance at 517 nm becomes weaker (Figure S27c, Supporting Information). Figure 3f shows that the DPPH scavenging ability of MPMP nanozymes could reach up to 93%, which is 1.38-fold that of MoS_2 nanosheets. Moreover, blue–green $ABTS^+$, which is oxidized by ABTS, was also applied to investigate the effect of MPMP on RNS scavenging owing to its characteristic absorbance at 734 nm (Figure S28, Supporting Information). The nitrogen radical from $ABTS^+$ could be eliminated by both MoS_2 and polydopamine; thus, the blue–green color is decolorized, and the absorbance at 734 nm decreases sharply. Statistically, the scavenging ability of MPMP nanozymes toward $ABTS^+$ is equal to that of MPM nanozymes ($p > 0.05$), but 1.52-fold higher than that of MoS_2 nanosheets ($p < 0.001$) (Figure 3f).

The PTIO assay was also performed to assess the ability of MPMP to scavenge ·N—O free radicals (Figure S29a, Supporting Information). The weaker absorbance at 557 nm indicates that PTIO radicals have been eliminated by the MPMP nanozyme due to its excellent antioxidation capacity (Figure S29b, Supporting Information), which is attributed to the synergistic functions of MoS_2 and PDA. Statistically, the significantly lower PTIO scavenging ability of MoS_2 nanosheets than that of MPM ($p < 0.05$) and MPMP ($p < 0.01$) (Figure S29c, Supporting Information) further implies that modification of Mg-doped PDA contributes to improving the antioxidases-mimicking activities of MoS_2-based artificial nanozymes.

The Mo^{6+}/Mo^{4+} redox couple could switch between each state in response to the reactive species,[26] which is conducive to the antioxidases-mimicking properties. For example, the decomposition of H_2O_2 into O_2 in the alkaline conditions could be accelerated in the presence of MoS_2 nanosheets, and the reduced Mo^{4+} could be oxidized to Mo^{6+} by H_2O_2 (Figure S30a, Supporting Information). Similar to the CAT-mimicking performances, the cycle process between Mo^{4+} and Mo^{6+} through electron transfer is vital for the SOD-mimicking performance (Figure S30b, Supporting Information). Moreover, both hydrogen atom donation and electron transfer–proton transfer promoted the transformation from catechol to o-quinone, thereby scavenging the ROS/RNS (Figure S30c,d, Supporting Information). Moreover, the quinone could obtain protons, which come from primary amine groups of polydopamine and proteins, and then transfers to the original state of catechol. On the other hand, the residual catechol groups after the release of Mg^{2+} could be chelated with cellular metal ions, thereby inhibiting the enzymatic activities and generation of ROS/RNS. Finally, the polysulfobetaine could serve as the sacrificial agent owing to the relative reactive methylene groups (Figure S30e, Supporting Information). Therefore, the decoration of polysulfobetaine could enhance the antioxidases-mimicking performance.

Based on the above antioxidases-mimicking properties of MPMP nanozyme, we systematically evaluated its biological potential as a ROS/RNS scavenger in RAW264.7 cells. Compared

to the control group, there is more ROS/RNS production inside macrophages after LPS induction, including ·OH, $O^{\cdot}{}_2^-$ and NO (Figure 3g; Figure S31, Supporting Information), and then, the overexpressed reactive species are scavenged by MPMP nanozyme owing to its antioxidases-mimicking activities. According to the quantitative analysis, the cellular expression of ·OH and NO treated with MPMP nanozyme is significantly lower than that of LPS group ($p < 0.05$) (Figure 3h). Overall, the inflammatory response of the macrophages is activated by LPS induction, and the cells produce overexpressed ROS/RNS. These reactive species are completely scavenged by MPMP nanozyme due to its excellent antioxidases-mimicking activities (Figure 3i).

In OA joints, three typical normal cells, including BMSCs, SMSCs, and chondrocytes, are affected by inflammatory cells. To mimic the OA environment, we designed a co-culture system to evaluate whether the MPMP nanozyme can mediate the fate of normal cells under inflammatory conditions (Figure S32a, Supporting Information), which is inspired by a previous study.[6] As shown in Figure S32b–d (Supporting Information), LPS-activated RAW264.7 cells have secreted some cytotoxic cytokines and ROS/RNS that cause cell death, demonstrating significantly reduced cell viability (21.78% for BMSCs, 63.14% for SMSCs, and 67.42% for chondrocytes). After adding MPMP nanozyme to the co-culture system, the cell viability increases significantly. With NIR irradiation, cell viability is further improved (79.24% for BMSCs, 97.97% for SMSCs, and 95.44% for chondrocytes). Multiple functions have contributed to these results synergistically. i) NIR-triggered heat generation promotes the self-decomposition of H_2O_2 and enhances the enzymatic activities; ii) the antioxidases-mimicking activities of MPMP nanozyme eliminate various ROS/RNS produced by macrophages; and iii) efficient O_2 supplementation improves the hypoxic microenvironment induced by an overactive inflammatory response, thereby enhancing the function of mitochondria to maintain normal biological activities.

2.5. Biocompatibility of MPMP Nanozyme

Biomaterial biocompatibility is one of the most important standards prior to in vivo or clinical applications. In addition to the osteogenic differentiation, numerous previous studies have confirmed that BMSCs have the potential to differentiate into chondrocytes, which are the only tissue cells to secrete ECM to maintain cartilage homeostasis.[37,38] SMSCs have the capacity in producing HA that regulates the viscosity of synovial fluid and the lubrication performance of cartilage.[22,39] Therefore, BMSC and SMSC were selected to evaluate the biocompatibility of MPMP nanozyme. CCK-8 assays demonstrate that both BMSCs and SMSCs proliferate well from 24 to 72 h when incubated with MPMP nanozyme (Figures S33a and S34a, Supporting Information), which is closed to the control group. Additionally, live/dead staining images show that most of the cells live and grows well (Figures S33b and S34b, Supporting Information). Although there are scattered dead BMSCs at 72 h, which appear mainly due to contact inhibition of excess cells in the limited areas, it can be ignored compared to the abundance of live cells. Cell morphology images exhibit well-spread F-actin and clear cell pseudopodia (Figures S33c and S34c, Supporting Information), which constitute the motion skeleton to promote cell movement and growth. Different from the normal BMSCs with obvious F-actin and nuclei, obvious green fluorescent signals have been appeared inside the BMSCs when incubated with FITC-labeled MPMP nanozyme, indicating that the prepared MPMP nanozyme could be uptaken by the cells (Figure S35, Supporting Information). LDH release assay is selected to investigate the integrity of cell membranes to distinguish normal cells from apoptotic/dead cells. As shown in Figure S36 (Supporting Information), both BMSCs and SMSCs incubated with MPMP nanozyme shows no difference in LDH release, indicating that the MPMP nanozyme does not induce acute cell apoptosis or cell death. Moreover, mild temperatures from the photothermal effect of MPMP nanozyme could also decrease LDH release, exhibiting the synergistic protective performances of antioxidases-mimicking activities and thermal effect. LPS-activated inflammation models were also evaluated for realistic OA microenvironments. Unlike the positive group, which exhibits obvious apoptotic BMSCs and SMSCs, almost no apoptosis-positive cells are observed in the MPMP and MPMP-NIR groups (Figure S37, Supporting Information). These results reveal that the MPMP nanozyme with or without NIR irradiation is biocompatible in normal/inflammatory conditions.

2.6. Biological Mechanism Inflammation Suppression and Chondrogenic Differentiation

We systematically elucidated the effect of MPMP nanozyme on BMSCs. RNA sequencing analysis (RNA-seq) was performed to investigate the difference in gene expression between the control and MPMP-NIR groups. Before RNA-seq analysis, we performed LPS induction for 24 h and MPMP-NIR treatment (10 min per day) for 7 days (**Figure 4**a). According to the results analyzed by the Novomagic platform, a total of 2005 differentially expressed genes (DEGs) ($|\log_2 \text{FoldChange}| > 1$; $p_{adj} < 0.05$) are identified after MPMP-NIR treatment (1203 for upregulated DEGs and 802 for down-regulated DEGs, respectively), with HSP 70, Col2a1 and IL-6 genes as representatives (Figure 4b). Furthermore, GO biological process enrichment analysis of DEGs was used to explore the associated functions of these genes. As shown in Figure 4c, there are obvious heat response performances ("heat generation"), antioxidation/anti-inflammation ("cellular response to ROS", "response to decreased oxygen level", and "oxidoreductase activity"), and chondrogenesis ("glycosaminoglycan binding" and "chondrocyte development" and "chondrocyte differentiation"), indicating that MPMP-NIR mediated thermal effect contributes to inhibition of inflammatory response and chondrogenic differentiation. Also, GO enrichment analysis of down-regulated DEGs shows that MPMP-NIR treatment can modulate inflammation response ("RNS metabolic process", "regulation of ROS metabolic process" and "regulation of inflammatory response"), which further convinces the antioxidases-mimicking performance of MPMP nanozyme involving in heat response performance ("response to temperature stimulus") (Figure S38, Supporting Information). Ulteriorly, KEGG enrichment analysis also confirms these results. The upregulated genes in KEGG enrichment analysis reveal that MPMP-NIR treatment involves in "Glycosaminoglycan biosynthesis", "IL-17 signaling pathway" and

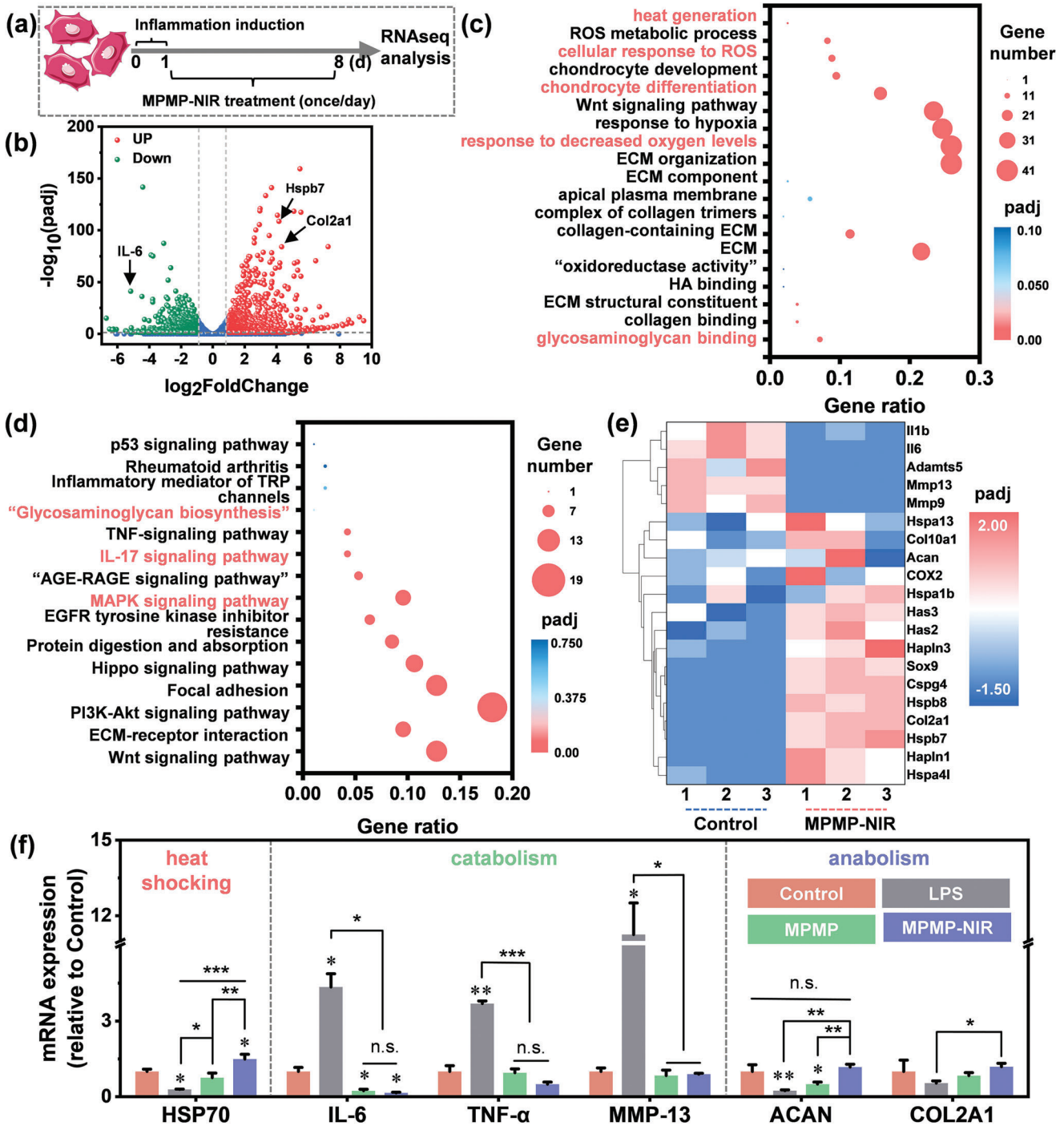

Figure 4. RNA sequencing analysis of BMSCs with LPS induction and MPMP-NIR treatment. a) Schemes of experimental design. b) Volcano plot of differentially expressed genes (DEGs) ($|\log_2 \text{FoldChange}| > 1$, padj < 0.05). c) GO and d) KEGG enrichment analysis of upregulated DEGs. e) Cluster heatmap of DEGs of interest which involve in heat generation, inflammation inhibition, and chondrogenic differentiation. The full description of these DEGs is listed in Table S4 (Supporting Information). f) Relative mRNA expression (HSP70, IL-6, TNF-α, MMP-13, ACAN and COL2A1). Data are shown as mean ± SD ($n = 3$). *($p < 0.05$) and **($p < 0.01$) indicate significantly difference in comparison with control group. *($p < 0.05$), **($p < 0.01$) and ***($p < 0.001$) implies statistical significance of the comparisons between other groups. n.s. ($p > 0.05$) suggests no significant difference. The full description "oxidoreductase activity" in (c) is "oxidoreductase activity, acting on the CH–NH_2 group of donors, oxygen as acceptor". The full descriptions of "Glycosaminoglycan biosynthesis" and "AGE-RAGE signaling pathway" in (d) is "Glycosaminoglycan biosynthesis-chondroitin sulfate/dermatan sulfate" and "AGE-RAGE signaling pathway in diabetic complications".

"MAPK signaling pathway" (Figure 4d). Meanwhile, KEGG enrichment analysis of the down-regulated DEGs are related to "NF-kappa B signaling pathway", "IL-17 signaling pathway", "Toll-like receptor signaling pathway", and "NOD-like receptor signaling pathway" (Figure S39, Supporting Information).[40] Furthermore, a heatmap of the selected genes of interest demonstrates that MPMP nanozyme with NIR irradiation could promote the expression of thermal effect-related genes (such as Hapln1, Hspa4l, Hspab7, and Hspa1b) and chondrogenic differentiation-related genes (Col2al, Cthrcl, Sox9, Cspg4, Has2, and Acan), and inhibit the expression of inflammation-related genes (IL1b, IL6, MMP13, MMP9, and Adamts5) (Figure 4e). The above results imply that the MPMP nanozyme with NIR irradiation could upregulate the photothermally mediated chondrogenesis and downregulated the inflammatory response, which is realized by the mild heat generation from the photothermal effect.

2.7. Chondro-Inducive and HAS-Mimicking Effect of MPMP Nanozyme under NIR Irradiation

According to RNA-seq analysis, MPMP nanozyme with NIR irradiation perhaps restores joint homeostasis by regulating heat shocking, catabolism, and anabolism. As for the heat shock reaction, the expression of HSP70 of LPS group is inhibited significantly ($p < 0.05$) compared with that of the control group, whereas the HSP70 level in MPMP group is equal to the control (Figure 4f). These data reveal that inflammatory response is the principal factor for inhibiting heat shock reaction, however, this side effects could be offset by the antioxidases-mimicking properties of MPMP nanozyme. Surprisingly, The MPMP-NIR group shows the highest HSP70 mRNA level ($p < 0.05$ for control, $p < 0.001$ for LPS, and $p < 0.01$ for MPMP, respectively), indicating that photothermal effect of MPMP nanozyme could activate the heat shocking effectively for self-defensive mechanism of cells. Due to the activated inflammatory response, the IL-6, TNF-α, and MMP 13 levels are 4.35-fold, 3.69-fold, and 11.25-fold to the control group, respectively. Whether applying NIR irradiation or not, MPMP nanozyme could inhibit the expression of inflammation-related and degradation-related genes, and the MPMP-NIR shows the lowest gene levels, indicating that the catabolism is mainly suppressed by the antioxidases-mimicking activities of MPMP nanozymes and the photothermal-mediated heat shocking has the enhanced effect on anti-inflammation. In terms of the anabolism, due to the inhibitory effect of inflammatory response on biosynthesis of glycosaminoglycan and Col II, LPS group shows reduced ACAN and COL2A1 levels in comparison to the control group. The ACAN level in MPMP is significantly lower than that of the control group ($p < 0.05$) and the COL2A1 level in MPMP group is just equal to that in the control group, suggesting that the intrinsic antioxidation effect of MPMP nanozyme itself could only inhibit the inflammatory response and have a limited effect on promoting chondrogenic ability. Surprisingly, MPMP-NIR shows the highest expression of ACAN and COL2A1. These results suggest that upregulation of HSP70 by mild photothermal performance could promote chondrogenic genes and inhibit the expression of inflammatory genes, which is also in accordance with antioxidases-mimicking activity of MPMP nanozyme mentioned above.

Protein secretion is also regarded as a direct method for exploring the chondrogenic differentiation of BMSCs. As shown in Figure S40 (Supporting Information), HSP-70 protein level is reduced by LPS induction, reversed by antioxidases-mimicking activity of the MPMP nanozyme and further enhanced by mild photothermal effect. Compared with the LPS group, there is a higher expression of aggrecan ($p < 0.01$) and Col II ($p < 0.001$,) in the MPMP-NIR group (Figure S41, Supporting Information). Similar to the aforementioned results, inflammation-related proteins (IL-6, PGE-2, and TNF-α) are overexpressed in the LPS group and gradually decreased in the MPMP and MPMP-NIR groups (Figure S42, Supporting Information). Immunofluorescent staining images in **Figure 5**a,b exhibits that the decreased expression of aggrecan and Col II in the LPS group could reach to equal levels to the control group when incubated with MPMP nanozyme. Surprisingly, MPMP-NIR not only retards the adverse effect of the inflammatory response, but also further accelerates the chondrogenic differentiation of BMSCs, which is demonstrated by the high fluorescence intensity of both aggrecan and Col II (Figure S43, Supporting Information). According to the results of Western Blot analysis, MPMP-NIR successfully activated the heat shock reaction of BMSCs in terms of the highly expressed HSP 70, then the levels of inflammation-related proteins (TNF-α, IL-6, MMP 13) caused by LPS have been inhibited. Moreover, the levels chondrogenic proteins (aggrecan and Col II) have been improved (Figure S44, Supporting Information).

In addition to aggrecan/Col II, HA, which is mainly secreted by synovial cells, is another major component in the articular cavity, supplying viscosity for synovial fluid and providing lubrication for cartilage. Previous studies have confirmed that HAS-2 is the major synthetic enzyme that regulates HA production;[25] thus, HAS-mimicking activity of artificial nanozymes to promote HA synthesis could be a popular candidate for cartilage regeneration, which has not yet been reported. In the current study, we hypothesized that the mild photothermal effect triggered Mg^{2+} release and HSP-70 expression could synergistically enhance HA production (Figure 5c). Similar to the above data, LPS treatment reduces the expression of HSP-70 inside SMSCs, whereas the treatment with MPMP and MPMP-NIR could deal with this dilemma (Figure 5d). Intracellular HA production in the MPMP-NIR group is significantly higher than that in other groups ($p < 0.05$ for control, $p < 0.01$ for LPS, and $p < 0.05$ for MPMP) (Figure 5e). Similarly, LPS induction suppressed the production of extracellular HA ($p < 0.001$), and that in MPMP group is maintained at the same level as the control group. Indeed, MPMP-NIR promotes rSMSCs to deposit more HA than other groups (Figure 5f). Overall, the obtained data provide cogent evidence for the HAS-mimicking activity of MPMP nanozyme with NIR irradiation.

The potential signaling pathways of HSP70 and Mg^{2+}, which are regulated by the photothermal performance of dual-bionic MPMP nanozyme, are established in Figure 5g. In an inflammatory microenvironment, the activation of NF-κB signaling pathways would induce overexpression of reactive species such as NO and $O^{\cdot}{}_2^-$, which suppressed the expression and activities of antioxidases (such as SOD and CAT). With the mediation of MPMP nanozyme under NIR irradiation, highly expressed HSP70 inhibits the activation of NF-κB signaling pathways and enhances the activities of SOD/CAT as molecular chaperone, then the

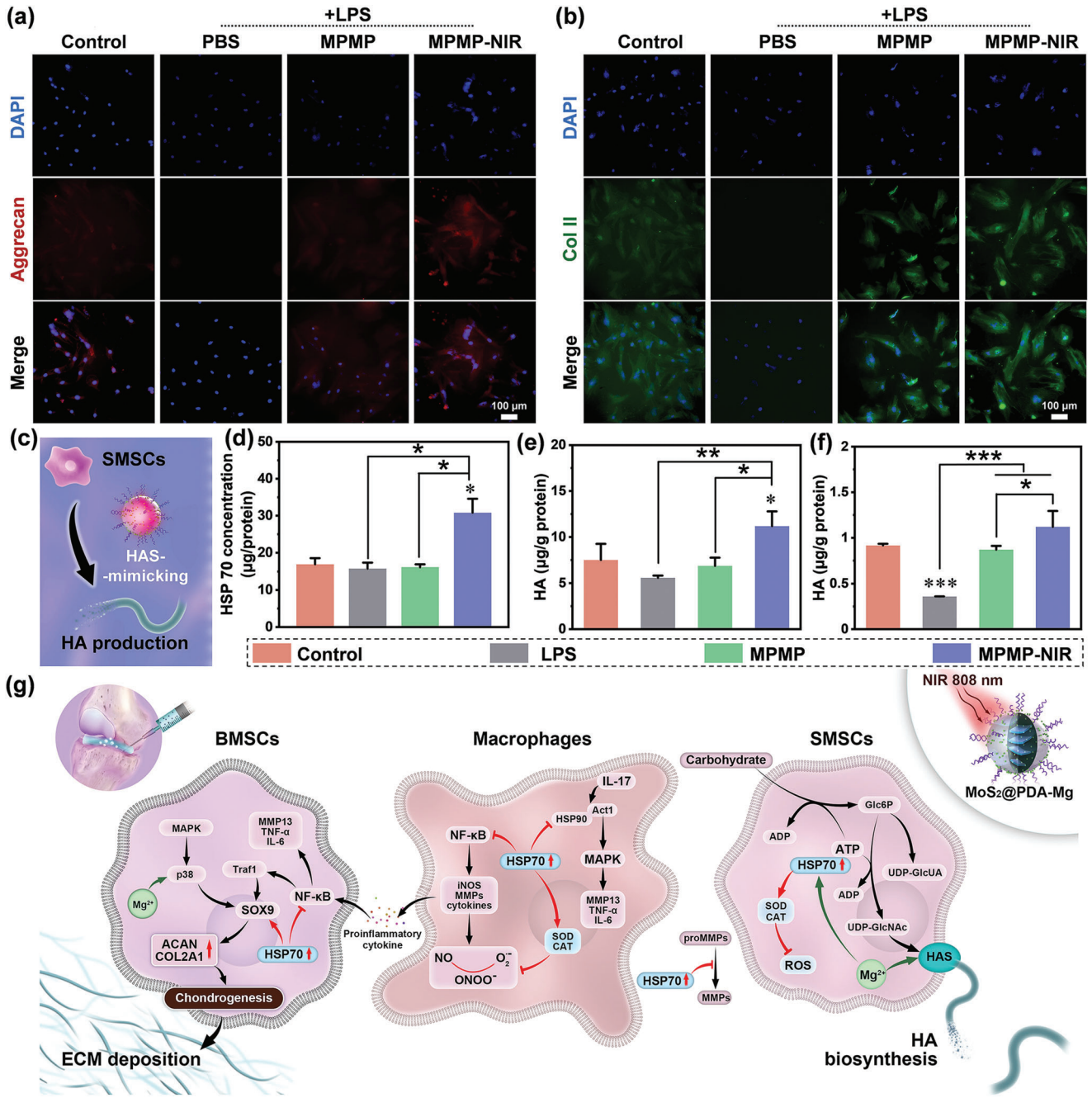

Figure 5. Chondrogenic induction of MPMP nanozyme toward BMSC and SMSC. a,b) Immunofluorescent staining of aggrecan (a) and Col II (b) of BMSCs. c) The scheme of HAS-mimicking activity of MPMP nanozyme with photothermal effect and d–f) corresponding HSP 70 expression (d) and intracellular (e) and extracellular (f) HA production. Data are shown as mean ± SD ($n = 3$). * ($p < 0.05$), ** ($p < 0.01$) and *** ($p < 0.001$) indicates a significant difference in comparison to the control group, * ($p < 0.05$), ** ($p < 0.01$) and *** ($p < 0.001$) suggests statistical difference between other groups. g) The scheme of signaling pathways of antioxidation/antiinflammation/chondrogenesis/HA biosynthesis of dual-bionic MPMP nanozyme under NIR irradiation, which exhibit great potential in OA therapy.

downstream genes related to inducible nitric oxide synthase (iNOS), MMPs and cytokines would be suppressed. Meanwhile, the ROS/RNS production could be reduced accordingly. On the other hand, activation of IL-17 signaling pathway finally induces the expression of inflammation-related genes (IL-6, MMP-13, and TNF-α), where HSP90 is vital for the actions of Act1. Owing to the antagonistic effect on HSP90, thermal-triggered HSP70 expression inhibit the biological actions of Act1, thereby suppressing the expression of downstream inflammatory genes. Therefore, the intrinsic antioxidases-mimicking properties of MPMP could eliminate intracellular/extracellular ROS/RNS, while NIR-induced HSP70 could further enhance its antioxidation and

anti-inflammation properties by an inhibitory effect on NF-κB and IL-17 signaling pathway.

The anabolic processes contain chondrogenic differentiation of BMSCs and HA production of SMSCs. The HSP70-induced chondrogenic differentiation of BMSCs manifests in two ways. i) It restrains the activation of NF-κB, and then inhibit the block effect of Traf1 on Sox9 and expression of MMP-13, TNF-α, and IL-6, which provide a better microenvironment for chondrogenesis. ii) It shows promotive effect on Sox9 and the Mg^{2+} could also improve the expression of Sox9 by regulating p38 genes, thus the downstream genes such as ACAN and COL2A1 are highly expressed. As for SMSCs, HSP70-enhanced enzymatic activities of SOD/CAT scavenge intracellular ROS/RNS, thereby reducing cell apoptosis/death and providing comfortable conditions for HA biosynthesis. The released Mg^{2+} controlled by photothermal performance of MPMP nanozyme could promote the binding of adenosine triphosphate (ATP) and HSP70, which enhances the conversion of ATP to adenosine diphosphate (ADP) and provides more energy for generation for HA sources (UDP-GlcNAc and UDP-GlcUA) from carbohydrates. Besides, Mg^{2+} also takes parts in HA production.[25b] Therefore, dual-bionic MPMP nanozyme, especially under NIR irradiation, shows tremendous potential in OA therapy.

2.8. MPMP Nanozyme with NIR Irradiation Relieves OA Pathological Process

The therapeutic effect of MPMP nanozyme under NIR irradiation was evaluated by I.A. injection (8 weeks, once per week) into the knee joints of OA mice after MIA induction (**Figure 6**a). OA with progressive cartilage degradation and damage is often characterized by articulate space narrowing and osteophytes appearance. As shown in the 2D images (Figure S45, Supporting Information) and reconstructed 3D images (Figure 6b,c; Figure S46, Supporting Information) of knee joints from Micro CT analysis, the articulate space width (ASW) is significantly decreased in the OA group ($p < 0.05$) compared with the normal group, and obvious osteophytes could be easily visualized around the boundary of the articular cartilage. In contrast, MPMP nanozyme can relieve OA pathological process by inhibiting articulate space narrowing and osteophyte formation; however, its therapeutic effect is still limited because of the significantly higher osteophyte volume than the normal group ($p < 0.05$), indicating that I.A. injection of MPMP nanozyme alone fails to prevent cartilage wear. With mild heat generation by the photothermal effect, osteophytes in the MPMP-NIR group are smaller and less than those in the OA and MPMP groups. Statistically, the ASW of the MPMP-NIR group is significantly higher than that of the OA group ($p < 0.01$) and equal to that of the normal group ($p > 0.05$), whereas the osteophyte volume is significantly smaller than that of OA group ($p < 0.05$) and MPMP group ($p < 0.01$). There is no significant difference in osteophytes between the MPMP-NIR and normal groups, indicating that MPMP nanozyme under NIR irradiation can restore the lubrication property of cartilage, alleviate joint degradation and damage, thus reducing the formation of osteophytes.

Restoring joint homeostasis involves cartilage regeneration and inflammation inhibition. The healthy cartilage shows a smooth and intact surface, standard gradient structure, and normal cell morphology (Figure 6d). However, owing to the cartilage degradation, lubrication dysfunction, and abnormal load transformation in the OA group, serve abrasion is observed on the cartilage surface, and abnormal cartilage structures accompanied by disorganized chondrocytes and narrowed cartilage width are also observed. Worse yet, the cartilage matrix, specifically aggrecan, and glycosaminoglycan, begins to disappear (Figures S47 and S48, Supporting Information). After treatment with MPMP nanozyme, the OA cartilage is partly healed, whereas the discontinuous rough surfaces and scattered defects still exist. With the supplement of the photothermal effect, the structures/compositions of cartilage in the MPMP-NIR group are similar to those in the normal group. More specifically, the reduced aggrecan expression in OA group has been greatly improved (Figure S49, Supporting Information). Owing to the HAS-mimicking property of MPMP nanozyme under NIR irradiation, the aggrecan expression of MPMP-NIR group is obvious. In addition, MPMP nanozyme has antioxidases-mimicking properties, which prevent cartilage from degradation by ROS/RNS and degradation enzymes. On the other hand, inhibition of inflammation response in joint is also an important index of OA therapy. H&E staining images of synovium exhibit that aggregated inflammatory cell can be only observed in OA group, while the other three groups show normal cell distribution (Figure S50, Supporting Information). Similarly, due to the severe inflammation, both cartilage and synovium in OA group display cells with positive expression of TNF-α (Figure S51, Supporting Information). Although it seems that cells in MPMP group don't show TNF-α expression, the structure of synovium is a little malformed, indicating that simple antioxidation therapy with lubrication performance could not reverse OA completely. With the addition of PTT, the TNF-α expression of MPMP-NIR group has no difference with the normal group. Moreover, OA group exhibits obvious MMP-13 expression in both cartilage and synovium (Figure S52, Supporting Information), which is regarded as one of the major factors of cartilage degradation. MPMP nanozyme shows MMP-13 expression in synovium instead of cartilage, while MPMP-NIR group exhibits no expression of MMP-13. The obtained data reveal that dual-bionic MPMP nanozyme with NIR irradiation has the best therapeutic effect on restoring joint homeostasis.

It is also noted that the OARSI score has increased significantly in the OA group ($p < 0.01$) in comparison to the normal group, and then statistically reduced by MPMP ($p < 0.05$) (Figure 6e) revealing that there is almost no loss of cartilage matrix, the injury area is less than 5%, and small areas of cartilage surface wears. With the MPMP-NIR treatment, a significant reduction (88.57%) in OARSI score has appeared ($p < 0.01$), which conforming the best efficacy in OA therapy and joint homeostasis restoration. As for the structures, matrix deposition, cell phenotypes, and total evaluation of cartilage repairing, the Mankin's scores of MPMP-NIR is significantly lower than those of OA groups, with 85.42% reduction in total score as representative; whereas there is statistical difference between MPMP group and the OA group in terms of structure and cell phenotype (Figure S53, Supporting Information), indicating that MPMP nanozyme with NIR irradiation provides superior therapeutic effect. In light of the cartilage damages, the ICRS score of OA group reaches up to 4, which

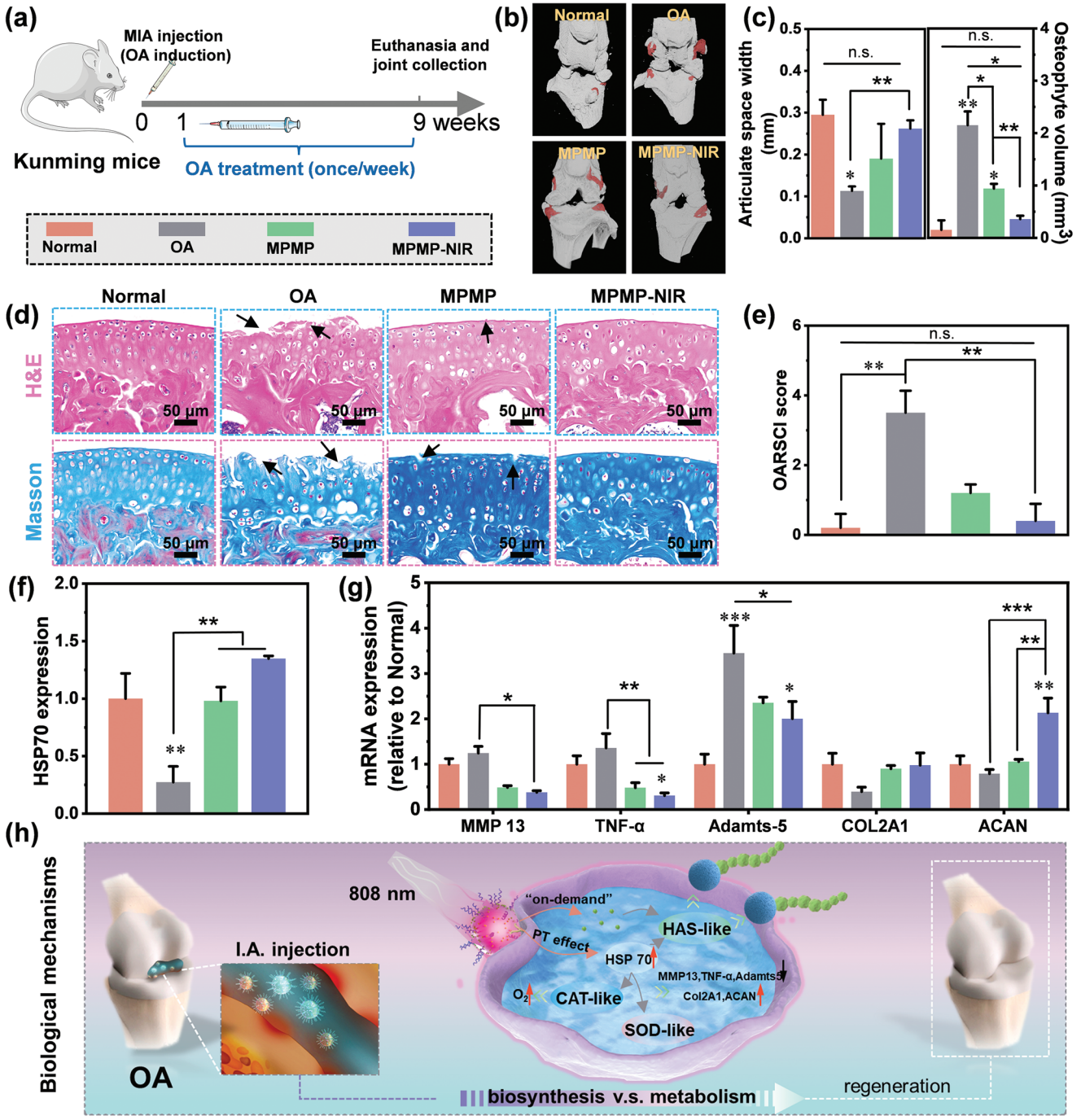

Figure 6. Therapeutic effect of MPMP nanozyme on MIA-induced OA mice without or with NIR. a) Experimental schedule of establishment of OA model and treatment with MPMP-NIR. b) Typical reconstructed 3D images of mice joints, and c) related articulate space and osteophyte volume. d) Histological staining slices (H&E staining and Masson staining) and e) OARSI score of Normal, OA, MPMP, and MPMP-NIR groups. f,g) RT-qPCR analysis of mRNA expression: f) HSP 70 and g) MMP 13, TNF-α, Adamts-5, COL2A1, and ACAN. h) Biological mechanism of MPMP nanozyme under NIR irradiation that mimics HAS and antioxidases (CAT and SOD) to regulate the balance between biosynthesis and metabolism, which finally realizes cartilage regeneration of OA joint. Data are shown as mean ± SD ($n = 5$). * ($p < 0.05$), ** ($p < 0.01$) and *** ($p < 0.001$) indicates a significant difference in comparison to the Control group, * ($p < 0.05$), ** ($p < 0.01$) and *** ($p < 0.001$) suggests statistical difference between other groups. n.s. ($p > 0.05$) implies that there is no significant difference.

is significantly higher than that of the normal group ($p < 0.05$) (macroscopic appearance, Figure S54, Supporting Information), indicating over 50% of injury in cartilage thickness under inflammatory and abnormal friction forces. MPMP groups exhibit reduced ICRS scores without statistical differences, whereas the MPMP-NIR group shows a significantly decreased ICRS score in comparison to the OA group ($p < 0.05$). Collectively, these results demonstrate that MPMP-NIR can relieve cartilage degradation and reconstruct cartilage structure, contributing to the regeneration of cartilage abrasion caused by OA.

To gain insight into biological mechanism of MPMP-NIR acting on OA therapy, RT-qPCR analysis has been performed. As shown in Figure 6f, a significant reduction in HSP70 mRNA expression in the articular cartilage is noted in the OA group compared to the normal group ($p < 0.01$). However, both MPMP and MPMP-NIR treatments can improve the mRNA expression of HSP70 compared to the OA group, indicating that antioxidases-mimicking activity could counteract the adverse effect of OA on suppressing HSP70 expression. With a mild photothermal effect, MPMP-NIR exhibits the highest HSP70 mRNA levels. The regulation of inflammation is also important for OA therapy. Compared with the OA group, the significantly sharp reduction in mRNA expression of MMP 13 ($p < 0.05$), TNF-α ($p < 0.01$), and Adamts-5 ($p < 0.05$) is remarkable in MPMP-NIR group (Figure 6g). Moreover, no difference is observed between the normal and MPMP-NIR groups, suggesting that dual-bionic MPMP nanozyme with NIR irradiation could totally prevent cartilage degradation. As for chondrogenic genes (COL2A1 and ACAN) that contribute to cartilage regeneration, MPMP-NIR shows the best promotive effect. In particular, ACAN mRNA expression in MPMP is significantly higher than that in the OA ($p < 0.001$), MPMP ($p < 0.01$), and even normal ($p < 0.01$) groups, indicating the renewal of aggrecan, such as HA, owing to the HAS-mimicking activity of MPMP-NIR treatment.

In order to evaluate the biosafety of dual-bionic MPMP nanozyme, the histological staining of major organs (Figure S55, Supporting Information) and routine blood examination (Table S5, Supporting Information) have been performed. All H&E staining images of major organs exhibit normal tissue morphology without any necrosis and degradation. Additionally, there is no aberrance of blood biochemical indexes. Therefore, it is noted I.A. injection of MPMP nanozyme along with NIR irradiation to treat OA is a biosafe measure.

Collectively, M and MPM nanozymes with weak antioxiadases-mimicking activities have failed in treating, which are discussed in Supporting Information in detail. Enhancement in antioxidation properties has improved the anti-inflammation effect of MPMP nanozyme, however, it exhibit deficiencies of chondrogenesis owing to its absence in HAS-mimicking activity. MPMP-NIR has the best capacity in regulating cartilage homeostasis, thereby alleviating cartilage degradation and delaying OA pathology.

The spatiotemporal OA therapy based on dual-bionic MPMP nanozyme involves three aspects. Firstly, the thermally enhanced lubrication property of MPMP nanozyme with NIR irradiation reduces the frictions that often cause cartilage wear. The hydration layer is easily formed by surface modification of zwitterionic polymer brushes,[41] which enables the slippery sliding of cartilage. The mild photothermal effect also provides sufficient energy for the sulfobetanie polymer chains of MPMP nanozyme to overcome the energy barrier of ionic–dipole interactions and hydrogen bonds, thereby improving the flexibility of the side chains, absorbing more water to generate a hydration layer, and further lowering the COF. Next, the antioxidases-mimicking activities of MPMP nanozyme inhibit the abnormal catabolism of OA, which could be also enhanced by the photothermal effect. As shown in Figure 6h, MPMP nanozyme exhibits SOD-mimicking and CAT-mimicking activities to scavenge ROS/RNS and supply O_2 for rescuing mitochondrial function.[42] With NIR irradiation, the MPMP nanozyme contributes to the upregulation HSP 70 expression, which could inhibit the activation of NF-κB and IL-17 signaling pathways, thereby enhancing the antioxidant effect to scavenge overproduced free radicals and suppressing the synthesis/secretion of inflammatory cytokines and degradation enzymes. Finally, the anabolism of OA joint is improved by the chondrogenesis and HA biosynthesis. On the one hand, the upregulated HSP70 expression inhibits the NF-κB signaling pathway and the on-demand release of Mg^{2+} enhances the MAPK signaling pathway, thus, BMSCs could differentiate into chondrocytes well even under inflammatory conditions. On the other hand, the released Mg^{2+} and the upregulated HSP 70 expression, which participate in biopolymerization of UDP-GlcUA/UDP-GlcNAc and the energy metabolism, contribute to amplifying the HAS-mimicking activity to produce HA synergistically, which has potential in restoring the viscosity of synovial fluid and replenish intrinsic lubrication performance. Thus, the expression of inflammation-related genes (MMP 13, TNF-α, and Adamts-5) is suppressed and chondrogenic genes (COL2A1 and ACAN) are increased. Therefore, MPMP-NIR weakens the adverse metabolism of OA and promotes the biosynthesis of chondrogenic processes, thus accelerating cartilage regeneration to alleviate OA.

3. Conclusion

Antioxidation and HA synthesis are important for relieving inflammation and promoting cartilage regeneration, thereby restoring the homeostasis of OA joints. Hence, the rational design of nanozyme to mimic antioxidases and HAS is desirable. In this study, we fabricated MPMP nanozyme to alleviate OA. Mild photothermal properties of the MPMP nanozyme improved the flexibility of PSB for enhancing hydration lubrication and regulating on-demand Mg^{2+} release to mimic HAS for HA generation. Effective scavenging of free radicals and O_2 supplementation under hypoxic conditions were realized by mimicking antioxidases. HSP 70 expression was upregulated to enhance ROS/RNS scavenging ability and promote HA biosynthesis and chondrogenesis, thereby treating OA effectively. Thus, this study not only demonstrated an MPMP nanozyme to mimic antioxidases and HAS at the same to treat OA, but also revealed that photothermally induced high expression of HSP70 is crucial for free radical scavenging, inflammation inhibition, and chondrogenesis, thereby exhibiting effective OA therapy.

4. Experimental Section

Details of materials and methods are available in the Supporting Information. All animal experiments were carried out with the

permission of Animal Research Committee of Sichuan University (approved No. KS2020028).

Supporting Information

Supporting Information is available from the Wiley Online Library or from the author.

Acknowledgements

This work was supported by the National Natural Science Foundation of China (No. 52073191, 51925304, and 51973133), and Sichuan Science and Technology Program (No. 2022NSFSC1949). The authors are grateful to Life Science Core Facilities (College of Life Sciences, Sichuan University) for the kind help in histological analysis. The authors thank Dr. Minghua Zhang (College of Polymer Science & Engineering, Sichuan University) for kind help with TEM characterization.

Conflict of Interest

The authors declare no conflict of interest.

Data Availability Statement

The data that support the findings of this study are available from the corresponding author upon reasonable request.

Keywords

dual-bionic nanozymes, hyaluronan synthase, lubrication replenishment, osteoarthritis, photothermal therapy

Received: April 9, 2023
Revised: July 7, 2023
Published online:

[1] W. Lin, J. Klein, *Adv. Mater.* **2021**, *33*, 2005513.
[2] a) B. G. Cooper, B. Catalina, A. Nazarian, B. D. Snyder, M. W. Grinstaff, *Biomaterials* **2018**, *181*, 210; b) P. Yu, Y. Liu, J. Xie, J. Li, *J. Controlled Release* **2021**, *338*, 486.
[3] T. V. Pereira, P. Juni, P. Saadat, D. Xing, L. Yao, P. Bobos, A. Agarwal, C. A. Hincapie, B. R. da Costa, *BMJ [Br. Med. J.]* **2022**, *378*, e069722.
[4] R. Xie, H. Yao, A. S. Mao, Y. Zhu, D. Qi, Y. Jia, M. Gao, Y. Chen, L. Wang, D. A. Wang, K. Wang, S. Liu, L. Ren, C. Mao, *Nat. Biomed. Eng.* **2021**, *5*, 1189.
[5] a) S. Brown, S. Kumar, B. Sharma, *Acta Biomater.* **2019**, *93*, 239; b) H. I. Pas, M. Winters, H. J. Haisma, M. J. Koenis, J. L. Tol, M. H. Moen, *Br. J. Sports Med.* **2017**, *51*, 1125.
[6] P. Yu, Y. Li, H. Sun, X. Ke, J. Xing, Y. Zhao, X. Xu, M. Qin, J. Xie, J. Li, *ACS Appl. Mater. Interfaces* **2022**, *14*, 27360.
[7] P. T. Newton, L. Li, B. Zhou, C. Schweingruber, M. Hovorakova, M. Xie, X. Sun, L. Sandhow, A. V. Artemov, E. Ivashkin, S. Suter, V. Dyachuk, M. El Shahawy, A. Gritli-Linde, T. Bouderlique, J. Petersen, A. Mollbrink, J. Lundeberg, G. Enikolopov, H. Qian, K. Fried, M. Kasper, E. Hedlund, I. Adameyko, L. Savendahl, A. S. Chagin, *Nature* **2019**, *567*, 234.
[8] N. Vanmuylder, L. Evrard, N. Dourov, *Anat. Embryol.* **1997**, *195*, 359.
[9] Q. W. Chen, X. H. Liu, J. X. Fan, S. Y. Peng, J. W. Wang, X. N. Wang, C. Zhang, C. J. Liu, X. Z. Zhang, *Adv. Funct. Mater.* **2020**, *30*, 1909806.
[10] M. T. Au, J. Shi, Y. Fan, J. Ni, C. Wen, M. Yang, *ACS Nano* **2021**, *15*, 11711.
[11] a) Y. Zhao, X. Peng, D. Wang, H. Zhang, Q. Xin, M. Wu, X. Xu, F. Sun, Z. Xing, L. Wang, P. Yu, J. Xie, J. Li, H. Tan, C. Ding, J. Li, *Adv. Sci.* **2022**, *9*, 2204535; b) L. Tan, Y. Hu, M. Li, Y. Zhang, C. Xue, M. Chen, Z. Luo, K. Cai, *Chem. Eng. J.* **2022**, *431*, 133382.
[12] a) Y. Li, P. Yu, J. Wen, H. Sun, D. Wang, J. Liu, J. Li, H. Chu, *Adv. Funct. Mater.* **2021**, *32*, 2110720; b) X. T. He, X. Li, M. Zhang, B. M. Tian, L. J. Sun, C. S. Bi, D. K. Deng, H. Zhou, H. L. Qu, C. Wu, F. M. Chen, *Biomaterials* **2022**, *283*, 121439; c) W. Qiu, W. Zhao, L. Zhang, H. Wang, N. Li, K. Chen, H. Zhang, Y. Wang, *Adv. Funct. Mater.* **2022**, *32*, 2208189.
[13] H. Cao, L. Yang, R. Tian, H. Wu, Z. Gu, Y. Li, *Chem. Soc. Rev.* **2022**, *51*, 4175.
[14] Y. Li, R. Fu, Z. Duan, C. Zhu, D. Fan, *ACS Nano* **2022**, *16*, 7486.
[15] A. Lin, S. Liu, H. Wei, *Particuology* **2023**, *76*, 32.
[16] Y. Zhao, Z. Zhang, Z. Pan, Y. Liu, *Exploration* **2021**, *1*, 20210089.
[17] M. Zandieh, J. Liu, *Adv. Mater.* **2023**, 2211041.
[18] a) F. Zhou, M. Li, M. Chen, M. Chen, X. Chen, Z. Luo, K. Cai, Y. Hu, *ACS Nano* **2023**, *17*, 4358; b) Y. Chen, Y. Wang, Z. Chen, J. Cai, K. Li, H. Huang, F. Song, M. Gao, Y. Yang, L. Zheng, J. Zhao, *Mater. Today Nano* **2022**, *19*, 100240; c) B. Liu, C. Li, G. Chen, B. Liu, X. Deng, Y. Wei, J. Xia, B. Xing, P. Ma, J. Lin, *Adv. Sci.* **2017**, *4*, 1600540; d) Y. Zhao, C. Wei, X. Chen, J. Liu, Q. Yu, Y. Liu, J. Liu, *ACS Appl. Mater. Interfaces* **2019**, *11*, 11587.
[19] W. Hou, C. Ye, M. Chen, W. Gao, X. Xie, J. Wu, K. Zhang, W. Zhang, Y. Zheng, X. Cai, *Bioact. Mater.* **2021**, *6*, 2439.
[20] L. Zhang, Z. Qin, H. Sun, X. Chen, J. Dong, S. Shen, L. Zheng, N. Gu, Q. Jiang, *Jiang, Bioact. Mater.* **2022**, *18*, 11.
[21] H. Xiong, Y. Zhao, Q. Xu, X. Xie, J. Wu, B. Hu, S. Chen, X. Cai, Y. Zheng, C. Fan, *Small* **2022**, *18*, 2203240.
[22] a) A. Singh, M. Corvelli, S. A. Unterman, K. A. Wepasnick, P. McDonnell, J. H. Elisseeff, *Nat. Mater.* **2014**, *13*, 988; b) A. Dodero, R. Williams, S. Gagliardi, S. Vicini, M. Alloisio, M. Castellano, *Carbohydr. Polym.* **2019**, *203*, 349; c) S. A. A. Isma Liza Mohd Isa, M. Kilcoyne, D. Sakai, P. Dockery, D. P. Finn, A. Pandit, *Sci. Adv.* **2018**, *4*, eaaq0597.
[23] F. P. Maloney, J. Kuklewicz, R. A. Corey, Y. Bi, R. Ho, L. Mateusiak, E. Pardon, J. Steyaert, P. J. Stansfeld, J. Zimmer, *Nature* **2022**, *604*, 195.
[24] L. J. Kang, J. Yoon, J. G. Rho, H. S. Han, S. Lee, Y. S. Oh, H. Kim, E. Kim, S. J. Kim, Y. T. Lim, J. H. Park, W. K. Song, S. Yang, W. Kim, *Biomaterials* **2021**, *275*, 120967.
[25] a) H. Li, H. Guo, C. Lei, L. Liu, L. Xu, Y. Feng, J. Ke, W. Fang, H. Song, C. Xu, C. Yu, X. Long, *Adv. Mater.* **2019**, *31*, 1904535; b) W. Wei, J. L. Faubel, H. Selvakumar, D. T. Kovari, J. Tsao, F. Rivas, A. T. Mohabir, M. Krecker, E. Rahbar, A. R. Hall, M. A. Filler, J. L. Washburn, P. H. Weigel, J. E. Curtis, *Nat. Commun.* **2019**, *10*, 5527; c) J. Ma, H. Cai, X. Long, K. Cheng, X. Xu, D. Zhang, J. Li, *Int. J. Biol. Macromol.* **2020**, *161*, 1011.
[26] T. Chen, H. Zou, X. Wu, C. Liu, B. Situ, L. Zheng, G. Yang, *ACS Appl. Mater. Interfaces* **2018**, *10*, 12453.
[27] H. Zhao, J. Li, H. Wu, T. Dong, Y. Zhang, H. Liu, *ChemElectroChem* **2018**, *5*, 383.
[28] D. Y. Zhang, Y. Zheng, H. Zhang, J. H. Sun, C. P. Tan, L. He, W. Zhang, L. N. Ji, Z. W. Mao, *Adv. Sci.* **2018**, *5*, 1800581.
[29] T. Hojo, M. Fujioka, G. Otsuka, S. Inoue, U. Kim, T. Kubo, *J. Orthop. Sci.* **2003**, *8*, 396.
[30] a) S. Chen, F. Yan, A. Zhong, L. Cai, *Cardiovasc Intervent Radiol* **2023**, *46*, 112; b) G. Kalamegam, M. Abbas, M. Gari, H. Alsehli, R. Kadam, M. Alkaff, A. Chaudhary, M. Al-Qahtani, A. Abuzenadah, W. Kafienah, A. Mobasheri, *Front. Physiol.* **2016**, *7*, 180.

[31] J. Ye, H. Haro, M. Takahashi, H. Kuroda, K. Shinomiya, *J. Orthop. Sci.* **2003**, *8*, 387.
[32] J. Chen, C. Li, S. Wang, *PLoS One* **2014**, *9*, e91561.
[33] X. Sun, X. He, Y. Zhu, E. Obeng, B. Zeng, H. Deng, J. Shen, R. Hu, *Chem. Eng. J.* **2023**, *451*, 138985.
[34] a) W. C. Jeong, S. H. Kim, S. M. Yang, *ACS Appl. Mater. Interfaces* **2014**, *6*, 826; b) B. Tian, C. Wang, Y. Du, S. Dong, L. Feng, B. Liu, S. Liu, H. Ding, S. Gai, F. He, P. Yang, *Small* **2022**, *18*, 2200786; c) S. Peng, H. Wang, Y. Xin, W. Zhao, M. Zhan, J. Li, R. Cai, L. Lu, *Nano Today* **2021**, *40*, 101240.
[35] a) G. Zhong, X. Yang, X. Jiang, A. Kumar, H. Long, J. Xie, L. Zheng, J. Zhao, *Nanoscale* **2019**, *11*, 11605; b) C. Zhao, J. Chen, J. Ye, Z. Li, L. Su, J. Wang, Y. Zhang, J. Chen, H. Yang, J. Shi, J. Song, *Angew. Chem., Int. Ed.* **2021**, *60*, 14458.
[36] S. Khan, D. Zhang, Y. Zhang, M. Li, C. Wang, *Mol. Cell. Endocrinol.* **2016**, *428*, 101.
[37] a) W. Shi, M. Sun, X. Hu, B. Ren, J. Cheng, C. Li, X. Duan, X. Fu, J. Zhang, H. Chen, Y. Ao, *Adv. Mater.* **2017**, *29*, 1701089; b) L. Zheng, S. Liu, X. Cheng, Z. Qin, Z. Lu, K. Zhang, J. Zhao, *Adv. Sci.* **2019**, *6*, 1900099.
[38] J. Zhou, Z. Zhang, J. Joseph, X. Zhang, B. E. Ferdows, D. N. Patel, W. Chen, G. Banfi, R. Molinaro, D. Cosco, N. Kong, N. Joshi, O. C. Farokhzad, C. Corbo, W. Tao, *Exploration* **2021**, *1*, 20210011.
[39] Q. Min, J. Liu, Y. Zhang, B. Yang, Y. Wan, J. Wu, *Pharmaceutics* **2020**, *12*, 613.
[40] X. Yan, B. Yang, Y. Chen, Y. Song, J. Ye, Y. Pan, B. Zhou, Y. Wang, F. Mao, Y. Dong, D. Liu, J. Yu, *Adv. Mater.* **2021**, *33*, 2104758.
[41] H. Chen, T. Sun, Y. Yan, X. Ji, Y. Sun, X. Zhao, J. Qi, W. Cui, L. Deng, H. Zhang, *Biomaterials* **2020**, *242*, 119931.
[42] F. Zhou, J. Mei, S. Yang, X. Han, H. Li, Z. Yu, H. Qiao, T. Tang, *ACS Appl. Mater. Interfaces* **2020**, *12*, 2009.